NACA RM L54C16

NACA

RESEARCH MEMORANDUM

EXPERIMENTAL EFFECTS OF PROPULSIVE JETS AND AFTERBODY CONFIGURATIONS ON THE ZERO-LIFT DRAG OF BODIES OF REVOLUTION AT A MACH NUMBER OF 1.59

By Carlos A. de Moraes and Albin M. Nowitzky

Langley Aeronautical Laboratory
Langley Field, Va.

NATIONAL ADVISORY COMMITTEE
FOR AERONAUTICS

WASHINGTON

April 22, 1954
Declassified April 15, 1958

NACA RM L54C16

NATIONAL ADVISORY COMMITTEE FOR AERONAUTICS

RESEARCH MEMORANDUM

EXPERIMENTAL EFFECTS OF PROPULSIVE JETS AND AFTERBODY CONFIGURATIONS ON THE ZERO-LIFT DRAG OF BODIES OF REVOLUTION AT A MACH NUMBER OF 1.59

By Carlos A. de Moraes and Albin M. Nowitzky

SUMMARY

The present investigation was made at a free-stream Mach number of 1.59 in order to compare the afterbody drags of a series of conical boattailed models at zero angle of attack. Afterbody drags were obtained for both the power-off and the power-on conditions.

Power-off boattail pressure distributions were compared with those predicted by the method of characteristics. The resultant boattail pressure drags were found to be 15 percent lower than those predicted by the characteristics theory. Measured base pressures were compared with values predicted by the method of Cortright and Schroeder and that of Love.

The interference effects of the propulsive jet on the boattail and base pressures were investigated as a function of boattail angle, jet pressure and Mach number ratio, and nozzle divergence angle.

The interference effects on the boattail pressure distribution were such as to always increase the pressure and hence decrease the drag. The base pressure was first decreased and then increased with increasing jet pressure ratio. Minimum base pressure and maximum base drag occurred at a jet pressure ratio near the ideal jet pressure ratio of 1.0. At the ideal jet pressure ratio, the base drag was from 33 to 110 percent more than in the power-off condition.

Low afterbody drag was found to be obtained with a high jet pressure ratio and nozzle divergence angle, some boattailing, and a low jet Mach number.

INTRODUCTION

In determining an aerodynamically efficient shape for a supersonic body or nacelle, careful consideration should be given to the afterbody configuration because its drag may be considerably higher than that of the forebody. To date, most of the test work and all of the theoretical advances have been made for the power-off condition, whereas relatively little work has been done in investigating afterbody configurations for the power-on condition.

Inasmuch as no theory has been advanced for determining the interference of a propulsive jet on the afterbody pressure distribution, total reliance must be placed on systematic studies of the parameters involved in determining the power-on afterbody pressure drag. One step in this direction is the investigation of the interference effects, from a systematic variation of the jet exit pressure and of the boattail angle, reported in reference 1. These tests were conducted at a Mach number of 1.91 with a "cold" air jet issuing from a convergent nozzle. Another step was taken in reference 2 which reports the jet interference effects on a parabolic body of revolution from a systematic variation of the jet-exit pressure. These tests were conducted at a Mach number of 1.92 with a "cold" air jet issuing from two convergent-divergent nozzles. Other jet interference effects have been observed for a rocket exhaust and are reported in references 3 and 4. Reference 5 is a summary of these and other data.

A rocket exhaust was used in the present investigation to determine the jet interference effects from a systematic variation of the boattail angle, jet nozzle half-angle, and the jet-exit pressure and Mach number. The models were cone-cylinder bodies with conical boattails. Boattail and base pressure distributions were obtained both with and without jet flow.

The present tests were conducted in the preflight jet of the Langley Pilotless Aircraft Research Station at Wallops Island, Va. The free-stream Mach number was 1.59 and the Reynolds number was 17.8×10^6, based on model length.

SYMBOLS

x body station, in.

l afterbody length, in.

d maximum body diameter, in.

L body length, in.

S area, sq in.

p static pressure, lb/sq in. abs

q dynamic pressure, lb/sq in. abs

H total pressure, lb/sq in. abs

M Mach number

C_p pressure coefficient, $\frac{p - p_o}{q_o}$

C_D pressure drag coefficient, $C_p \frac{S}{S_{max}}$

β boattail angle, deg.

λ jet nozzle half-angle, deg.

γ ratio of specific heats

Subscripts:

o free stream

j propulsive jet exit

b base

bt boattail

AB afterbody

MODELS

The three models used in this investigation are shown in figure 1. They are cone-cylinder bodies and two of them have conical boattail sections. All models have a 10° half-angle conical nose. The boattail angles are 0°, 5°, and 10° on models 1, 2, and 3, respectively. All models are 18.90 inches long with a fineness ratio of 7.87.

Afterbody pressure distributions were measured at the orifices shown on the line sketches of the afterbody configurations (fig. 2).

Jet nozzles of 0°, 11°, and 22° half-angles, shown in figure 2, were used in the present tests. Nozzle 1 ($\lambda = 0°$) was designed from the characteristics theory to have totally axial flow at the exit. Nozzles 2, 3, and 4 are merely conical sections from the throat to the exit.

The solid propellant used in this investigation was a Mk 12 grain modified with a taper at one end to produce regressive burning. In this manner a variation in jet-exit pressure was obtained with each test. The ratio of specific heats (γ) for the gas generated from burning this propellant was 1.22 and the stagnation temperature was approximately 4,000° R. The exit Mach number, calculated from the nozzle expansion ratio, was 2.65 for nozzles 1, 2, and 3; for nozzle 4, the Mach number was 2.16.

A sketch of the assembled model, prior to testing, is shown in figure 3.

TESTS AND INSTRUMENTATION

A detailed description of the preflight jet used in this investigation is given in reference 6. The present tests were conducted in the 27- by 27-inch jet at a Mach number of 1.59. The stagnation temperature was approximately 780° R and the free-stream static pressure was standard sea level. The Reynolds number was 17.8×10^6, based on model length.

A photograph of a typical setup prior to a test is shown as figure 4. In order to have the model completely within the Mach diamond of the free jet and to meet the interference criteria presented in references 7 and 8, the nose of the model was placed 8 inches upstream of the jet exit.

Pressure measurements on the model and of the tunnel conditions were obtained with electrical pressure pickups of the strain-gage type. Free-stream stagnation temperature was measured with an iron-constantan thermocouple. All data were recorded by oscillographs. Shadowgraphs were made of all tests and were time correlated with the pressure data.

Estimated accuracies of the test parameters are given in the following table:

Free-stream Mach number, M_o	±0.03
Pressure coefficient, C_p	±0.005
Jet pressure ratio, p_j/p_o	±0.03

RESULTS AND DISCUSSION

Prior to the test program, a study was made to determine the parameters involved in the jet interference problem and which of these parameters could be most readily studied with the preflight jet at Wallops Island. Accordingly, the present tests were arranged to study the jet interference effects, on the external pressure distribution of a body of revolution, as a function of: (a) the jet pressure ratio, p_j/p_o; (b) the boattail angle, β; (c) the jet nozzle half-angle, λ; and (d) the jet-exit Mach number, M_j.

The results of the present tests are presented as pressure distributions and pressure drag. No attempt has been made to include the friction drag because it would vary with the Reynolds number and heating conditions of a particular flight plan.

Power Off

Boattail pressures.- Boattail power-off pressure distributions were determined theoretically by the method of characteristics (ref. 9) and are presented in figure 5(a) as pressure coefficient plotted against axial distance from the model nose. Experimentally determined pressure distributions, which were obtained over the afterbody sections only, are also shown for purposes of comparison.

The pressures measured on the afterbody of model 1 show a trend dissimilar to theory. Although positive pressures on cylindrical afterbodies have been reported before which seem to substantiate the measurement at station 0.947, the measurements on the afterbody of model 1 were too few to either substantiate or reject the theoretical pressure distribution even though the large drop-off of pressure at station 0.992 was not predicted by theory. This sudden decrease in pressure is due to the location of the orifice in the expansion field of the flow as it turns the corner of the base.

The theoretical pressure distributions for models 2 and 3 correctly predict the increase in expansion and in the boattail pressure gradient with increasing boattail angle. However, for both models the predicted expansion was too large. The measured pressure distribution over the boattail of model 2 ($\beta = 5^\circ$) was parallel to, but less negative than, the theoretical pressure distribution. The pressure measurement at station 0.997 was not made in the present tests but was obtained on an identical model tested at the same Mach number. Here again a pressure orifice, located within the expansion field at the base, measured a pressure that was considerably lower than that which would be expected from an extrapolation of the measurements in the present tests.

The three pressure orifices on the boattail of model 3 ($\beta = 10^{\circ}$) were not sufficient to give a good pressure distribution. As in the case of the rearmost orifices of models 1 and 2, the orifice at station 0.992 read considerably lower than the theoretical value at that station. In view of the fact that the measured distribution over the boattail of model 2 was parallel to the theoretical distribution, a curve was drawn through the measured pressures, at stations 0.924 and 0.950 parallel to the theoretical boattail pressure distribution.

Integrating the pressure distributions results in the curve of the boattail drag coefficient shown in figure 5(b). The method of characteristics yielded drag coefficients that were consistently high, 15 percent for model 2 and 16 percent for model 3.

Base pressures.- Measured base pressure coefficients are presented in figure 6 as a function of boattail angle. Base pressure coefficients determined by the methods of references 1 and 10 are also shown for purposes of comparison. The method of reference 1 gave excellent agreement (within 5 percent) with the present test results, whereas the method of reference 10 indicated correctly the increase in base pressure with increasing boattail angle but predicted base pressures considerably higher than the measured values.

The base pressures measured in the present tests were lower than most of the available data. The present tests were conducted at a relatively high Reynolds number, however, with a turbulent boundary layer obtained from natural transition; whereas most other investigations have been conducted at a lower Reynolds number with either natural or artificial transition. Either natural transition at a lower Reynolds number or an artificially induced transition would tend to produce a thicker turbulent boundary layer, at the base, with an accompanying increase in base pressure.

Several investigations (for example, ref. 11) have shown that artificial transition produces base pressures 5 to 10 percent higher than that for natural transition, the larger differences being at the lower Mach numbers. It has also been shown many times (for example, ref. 7) that there is a decrease in base pressure with increasing Reynolds number, when the boundary layer just ahead of the base is turbulent. Application of these corrections, where applicable, results in good agreement between the present data and existing data.

Another factor which might affect the base pressure is the presence of the supporting strut. This strut is 6.25 percent thick in the streamwise direction and is tapered from a 4-inch chord at the model to a 10.5-inch chord at the base. At the model, the trailing edge is $1\frac{1}{2}$ chords forward of the base. Although not strictly applicable, because of the

taper and sweep of the strut, the analysis and data of reference 12 indicate that the effect of the strut on the base pressure would be very small. This is in agreement with the tests of reference 13 in which the rearward position of the side strut closely approximates the conditions of the present tests. At the higher Reynolds numbers used in the reference tests, the curves of measured and interference-free base drags converge. The side support strut is therefore believed to have had only a small effect, if any, on the results of the present tests.

Afterbody drag.- Combining the measured boattail and base drags yields the power-off afterbody drag coefficients shown in figure 7 as a function of afterbody fineness ratio. Increasing the afterbody fineness ratio from 0 to 1.92 results in a 50-percent reduction in afterbody drag, and further increases in afterbody fineness ratio will result in further decreases in the afterbody pressure drag. The theoretical methods of references 1 and 9 predict the afterbody drag well.

Power On

Boattail pressures.- Power-on boattail pressure distributions for models 2 and 3 are shown in figure 8 as pressure coefficient plotted against axial distance from the nose. The afterbody pressures on model 1 ($\beta = 0^\circ$) were not affected by the jet flow.

For model 2 ($\beta = 5^\circ$), the jet flow had no effect on the afterbody pressures except when the jet exhausted from nozzle 3 ($\lambda = 22^\circ$), and then only for jet pressure ratios greater than 2.1. The effect of the jet was to increase the boattail pressures in the vicinity of the base resulting in a decrease in the boattail drag. However, the area involved is small so that, except for very high jet pressure ratios, the drag savings would be small indeed. This reduction may be seen in figure 9 which shows the ratio of the power-on to the power-off boattail pressure drag as a function of the jet pressure ratio (defined as the ratio of jet-exit static pressure to free-stream static pressure).

As with model 2 ($\beta = 5^\circ$), the jet flow had no effect on the boattail pressures of model 3 ($\beta = 10^\circ$) except when it exhausted through nozzle 3 ($\lambda = 22^\circ$). However, for this model, the jet interference first occurred at a jet pressure ratio of 1.30 - much lower than it first occurred on the boattail of model 2. The ratio of jet to base diameter and jet to free-stream Mach number and the jet flow angles were the same for both of these models. Also, the jet mass flows were equal for the same jet pressure ratio. Hence, the underlying difference in the jet interference on these two models must be in the boattail angle, that is, the flow direction and Mach number at the end of the model.

That the drag reduction due to jet interference on model 3 ($\beta = 10^\circ$) is more significant than that on model 2 ($\beta = 5^\circ$) can be seen in figure 9. At a jet pressure ratio of 2.4, the reduction in boattail drag on model 3 was more than 16 percent of the power-off drag; whereas, on model 2, the reduction was only 1 percent of its power-off drag. Inasmuch, as the power-off boattail drag on model 3 is more than twice that on model 2, however, the more favorable interference effects of the jet still do not warrant its choice from a drag standpoint.

In an effort to gain a feel for the effect of the ratio of jet to free-stream Mach number, a fourth nozzle ($\lambda = 11^\circ$) was tested in model 3. This nozzle had the same exit area as the other nozzles, but had a larger throat so that the exit Mach number was 2.16 compared with 2.65 for nozzles 1, 2, and 3. Thus, for a given jet pressure ratio, the mass flow was less from this nozzle than from the other three.

The interference effects of the $M = 2.16$ jet on the boattail pressures and drag of model 3 ($\beta = 10^\circ$), may be seen in figures 8(c) and 9, respectively. As in the other cases where the boattail pressure distribution was disturbed by the propulsive jet, only the orifice closest to the base registered any change from its power-off reading. In this case, this orifice registered an increase when the jet pressure ratio exceeded 0.8. When nozzle 2 ($\lambda = 11^\circ$) was tested in this model, there were no interferences with the boattail pressure distribution even at the highest jet pressure ratio. Apparently then, there is an increasing interference from the jet as the ratio of jet to free-stream Mach number is decreased. This trend was also noted in reference 2 at a free-stream Mach number of 1.92.

A comparison of the interference effects from nozzle 3 ($\lambda = 22^\circ$) and nozzle 4 ($\lambda = 11^\circ$) is given in figure 9. At jet pressure ratios near the ideal pressure ratio of 1.0, a greater drag reduction is available from the jet of lower Mach number even though its divergence angle is but half that of the jet of higher Mach number. Above a jet pressure ratio of 1.6, the greater jet expansion from nozzle 3 results in greater jet interference on the boattail and consequently a greater pressure drag reduction. However, one might surmise that an even larger boattail drag reduction might be available if the divergence angle of nozzle 4 were 22° instead of 11°.

A comparison of nozzles 3 ($\lambda = 22^\circ$) and 4 ($\lambda = 11^\circ$) on the basis of the ratio of the total pressure to the free-stream static pressure in figure 10 shows that the nozzle of lower Mach number (nozzle 4) always produced the larger boattail drag reduction. This larger boattail drag reduction was accomplished despite the fact that the divergence angle of the nozzle was but half that of the nozzle with the higher Mach number.

Base pressure.- Base-pressure variations with jet pressure ratio are shown in figure 11. Power-off base-pressure coefficients are shown, for purposes of comparison, at the ratio of power-off base pressure to

free-stream static pressure. Inasmuch as the jet-exit pressure was computed from the measured combustion-chamber pressure, no attempt was made to correlate the data while the nozzle flow was in the separated condition. Thus, the curves of figure 11 begin at the point where the nozzle flow attaches.

At this flow-attaching pressure, the base pressures of all of the models are higher than their respective power-off values. For model 1, the increase in base-pressure coefficient was 0.025, whereas for models 2 and 3 the increase was approximately 0.04. As the jet pressure increased from the flow-attaching condition, the base pressure decreased until for model 1 it was 0.175 less than the power-off value. For models 2 and 3, the base pressures had decreased to approximately 0.125 less than their respective power-off values. These reductions in base pressure amount to increases in the base annulus drag of 192 percent, 209 percent, and 237 percent on models 1, 2, and 3, respectively. Further increases in the jet pressure ratio result in an increase in base pressure.

For model 1, the jet pressure ratios of the present tests were not high enough to result in the base pressure ever returning to its power-off value regardless of the nozzle half-angle. With models 2 and 3, however, the base-pressure increase with jet pressure ratio was sufficient to raise the base pressure to equal or exceed its power-off value by a pressure ratio of 2 for all nozzle half-angles. When nozzle 3 ($\lambda = 22^{\circ}$) was used in models 2 and 3, the base pressure returned to its power-off value at a jet pressure ratio slightly above the ideal pressure ratio of 1.0.

As shown in figure 12, nozzle 4 produced the same base-pressure trends with jet pressure ratio as had the other nozzles. Shown also, for comparison purposes, are two curves from figure 11(c). At a given jet pressure ratio, the highest base-pressure coefficient was obtained with the highest nozzle divergence angle at the higher jet Mach number. However, because of this difference in jet Mach numbers, the total pressures of the two jets would be very different. Figure 13 illustrates the more practical case where an engine produces a given jet total pressure and the choice of an exhaust nozzle must be made. Viewed in this manner the lower Mach number jet induces considerably less drag than the higher Mach number jet with the same divergence. It is also superior (from a drag standpoint) to the higher Mach number jet with twice the nozzle divergence.

The physical phenomenon which results in these large pressure changes may be seen in the shadowgraphs presented as figure 14. The large drop in base pressure between the nozzle starting pressure ratio and 0.8 is due to the aspiration or ejection effect of the propulsive and external flows on the low-energy boundary-layer air which flows into the "dead air" region around the annulus. Increasing the jet pressure increases the ejection of the air from the dead-air region. Because the flow into this region is not increased, the external and the jet flows must turn

more sharply towards the dead-air region with the result that the wake shock moves closer to the base. This increase in turning angle of the external flow increases its expansion and hence results in a decrease in the base pressure. At the same time, the wake shock becomes stronger as it moves towards the base. The increasing pressure gradient from the wake shock slows down the ejection action and the expanding jet begins to compress the dead-air region. In order to equalize the pressure in the external stream, the expansion from the boattail is reduced. When, because of the increase in jet pressure, the external flow over the dead-air region has the same inclination to the body center line as the boattail (that is, no expansion at the base), a further increase in jet pressure will result in a compression of the external flow at the base and the appearance of a lambda leg ahead of the main wake shock, as shown in figure 14(b). Further increases in the jet pressure result in the strengthening of these shocks and the continuation of their forward movements.

Afterbody drag.- Combining the measured power-on boattail and base drags results in the curves of afterbody drag coefficients presented in figure 15. Each set of curves is for a constant jet pressure ratio. Also included in this figure are the curves for the power-off afterbody drag (for which only the annulus drag has been used as the base drag so that comparison with the power-on curves will be on an equiarea basis). These curves show that, in the power-on condition, even more than in the power-off condition, the proper choice of afterbody configuration is of prime importance for low drag. It is also apparent that drag as well as thrust considerations should determine the nozzle configuration and operating pressures. At a jet pressure ratio of 0.8, the drag of the afterbody with a fineness ratio of 1.91 was from 30 to 50 percent higher with the power on than with the power off, depending on the nozzle half-angle. At a pressure ratio of 2.00, however, the drag of the same afterbody was from 0 to 47 percent lower than with the power off, again depending on the nozzle half-angle.

Comparison of the trends of the power-on and power-off curves, indicates that a large drag penalty must be paid for the use of low fineness ratio afterbodies.

The afterbody drag coefficients from the tests of nozzle 4 are shown in figure 16 as a function of jet pressure ratio.

Figure 17 presents a comparison of the interference effects from nozzles 2 ($\lambda = 11^\circ$), 3 ($\lambda = 22^\circ$), and 4 ($\lambda = 11^\circ$) on the afterbody drag of model 3 ($\beta = 10^\circ$). Above a pressure ratio of 15, the combination of low nozzle divergence and low jet Mach number produces the least drag. With a fixed nozzle expansion, the higher divergence angle has less afterbody drag. However, an even more important gain was realized by lowering the expansion ratio of the nozzle and hence the jet Mach number.

In the final analysis, the drag reductions made possible by the proper choice in afterbody configuration and jet operating parameters must be weighed against any changes in thrust and weight these choices bring about. Increasing the afterbody fineness ratio decreases the afterbody drag, increases the useful volume in a configuration, and increases the weight. Lowering the jet Mach number produces less thrust, as well as less drag, unless the mass flow can be increased by a corresponding amount (which would result in further gains). Increasing the jet pressure ratio for a constant combustion-chamber pressure decreases the thrust as well as the drag, and increasing the nozzle divergence angle decreases the thrust, drag, and weight.

The choice is not a simple one but in designing afterbody configurations due consideration must be given the power-on flight condition or serious penalties may result.

CONCLUDING REMARKS

The present investigation was made at a free-stream Mach number of 1.59 to compare the power-off and power-on afterbody drags of a series of conical boattail models at zero angle of attack.

The boattail and base pressures were measured and compared with theoretical predictions for the nonthrusting condition. The method of characteristics predicted boattail pressure drags that were 15 percent too high because the initial expansions from the cylindrical section to the conical boattails were not as severe as predicted. It was also found that the base pressures could be predicted within 5 percent.

Interference effects of the jet flow on the base pressure were found to either increase or decrease the base drag depending on the boattail angle, nozzle divergence angle, jet pressure ratio, and jet Mach number. These variables affected the base pressure in the following manner:

(1) Increasing the boattail angle from 0° resulted in an increase in base pressure. However, boattail angles of 5° and 10° yielded essentially the same base pressures.

(2) Increasing the nozzle divergence angle from 0° to 22° resulted in an increase in base pressure; the largest gain was from 11° to 22°.

(3) At the ideal pressure ratio of 1.0, the interference effects of the jet produced near-minimum base pressure and hence near-maximum base drag.

(4) For a given operating condition (constant total pressure), reducing the jet Mach number from 2.65 to 2.16 resulted in a higher base pressure than with the high Mach number jet at twice the divergence angle.

Positive base pressures were obtained with either a combination of boattailing, high jet pressure, and high nozzle flow divergence and Mach number, or a combination of boattailing, high jet pressure, and lower nozzle divergence and Mach number.

Interference effects of the jet flow on the boattail pressure distribution were found to exist only over the last 5 percent of the body length. The previously mentioned parameters affected the boattail pressures in the following manner:

(1) Increasing the boattail angle, the nozzle divergence angle, and the jet pressure ratio all resulted in an increase in the jet interferences effects.

(2) At a given engine operating condition, decreasing the jet Mach number from 2.65 to 2.16 was the most important change in decreasing the boattail drag.

Langley Aeronautical Laboratory,
National Advisory Committee for Aeronautics,
Langley Field, Va., February 25, 1954.

REFERENCES

1. Cortright, Edgar M., Jr., and Schroeder, Albert H.: Investigation at Mach Number 1.91 of Side and Base Pressure Distributions Over Conical Boattails Without and With Jet Flow Issuing From Base. NACA RM E51F26, 1951.

2. Love, Eugene S.: Aerodynamic Investigation of a Parabolic Body of Revolution at Mach Number of 1.92 and Some Effects of an Annular Jet Exhausting From the Base. NACA RM L9K09, 1950.

3. Gillespie, Warren, Jr.: Jet Effects on Pressures and Drags of Bodies. NACA RM L51J29, 1951.

4. Purser, Paul E., Thibodaux, Joseph G., and Jackson, H. Herbert: Note on Some Observed Effects of Rocket-Motor Operation on the Base Pressures of Bodies in Free Flight. NACA RM L50I18, 1950.

5. Cortright, Edgar M., Jr., and Kochendorfer, Fred D.: Jet Effects on Flow Over Afterbodies in Supersonic Stream. NACA RM E53H25, 1953.

6. Faget, Maxime A., Watson, Raymond S., and Bartlett, Walter A., Jr.: Free-Jet Tests of a 6.5-Inch-Diameter Ram-Jet Engine at Mach Numbers of 1.81 and 2.00. NACA RM L50L06, 1951.

7. Chapman, Dean R.: An Analysis of Base Pressure at Supersonic Velocities and Comparison With Experiment. NACA Rep. 1051, 1951. (Supersedes NACA TN 2137.)

8. Love, Eugene S., and O'Donnell, Robert M.: Investigations at Supersonic Speeds of the Base Pressure on Bodies of Revolution With and Without Sweptback Stabilizing Fins. NACA RM L52J21a, 1952.

9. Ferri, Antonio: Application of the Method of Characteristics to Supersonic Rotational Flow. NACA Rep. 841, 1946. (Supersedes NACA TN 1135.)

10. Love, Eugene S.: The Base Pressure at Supersonic Speeds on Two-Dimensional Airfoils and Bodies of Revolution (With and Without Fins) Having Turbulent Boundary Layers. NACA RM L53C02, 1953.

11. Reller, John O., Jr., and Hamaker, Frank M.: An Experimental Investigation of the Base Pressure Characteristics of Nonlifting Bodies of Revolution at Mach Numbers From 2.73 to 4.98. NACA RM A52E20, 1952.

12. Spahr, J. Richard, and Dickey, Robert R.: Effect of Tail Surfaces on the Base Drag of a Body of Revolution at Mach Numbers of 1.5 and 2.0. NACA TN 2360, 1951.

13. Perkins, Edward W.: Experimental Investigation of the Effects of Support Interference on the Drag of Bodies of Revolution at a Mach Number of 1.5. NACA TN 2292, 1951.

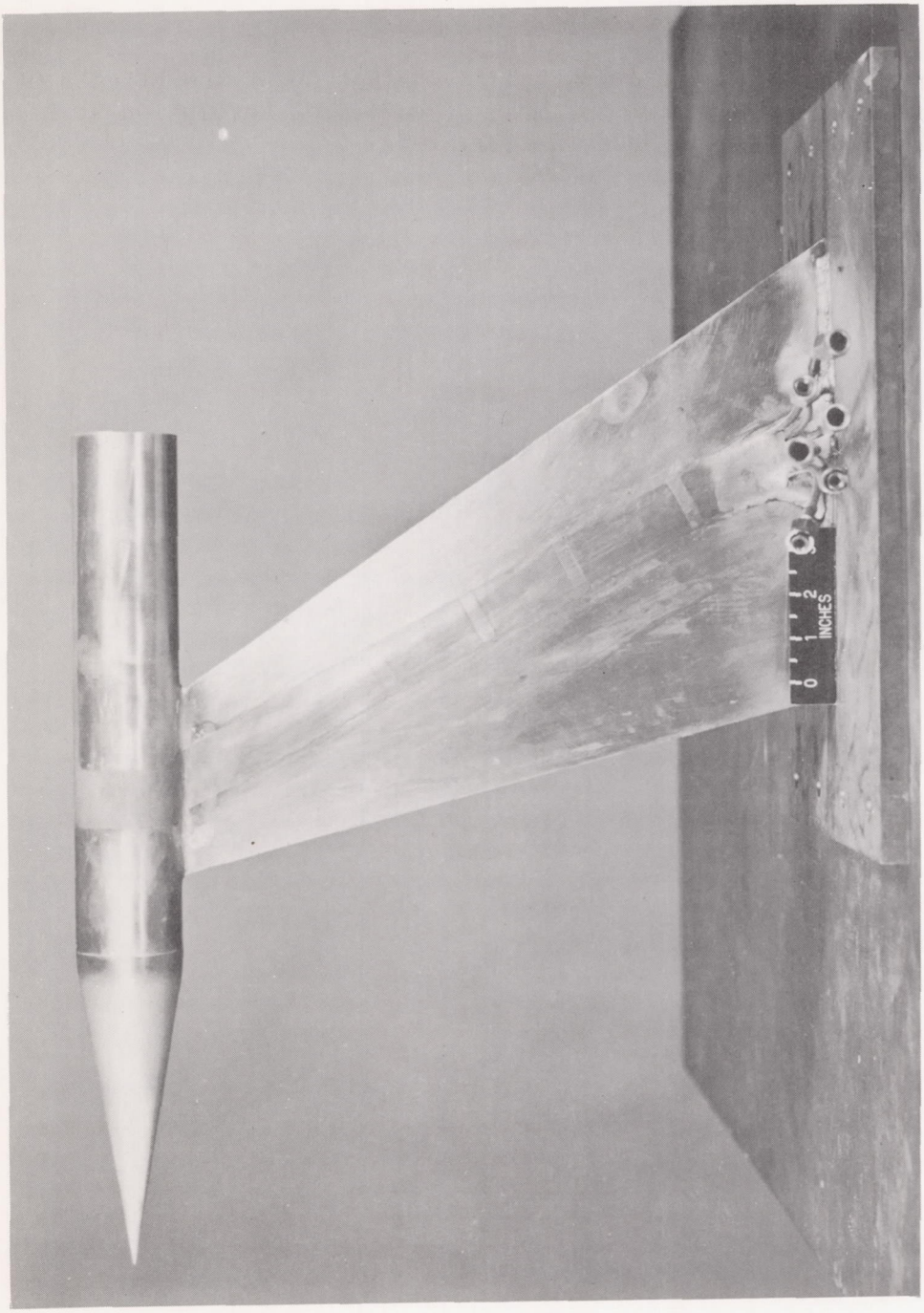

L-83172

(a) Model 1; $\beta = 0^{\circ}$.

Figure 1.- Test models.

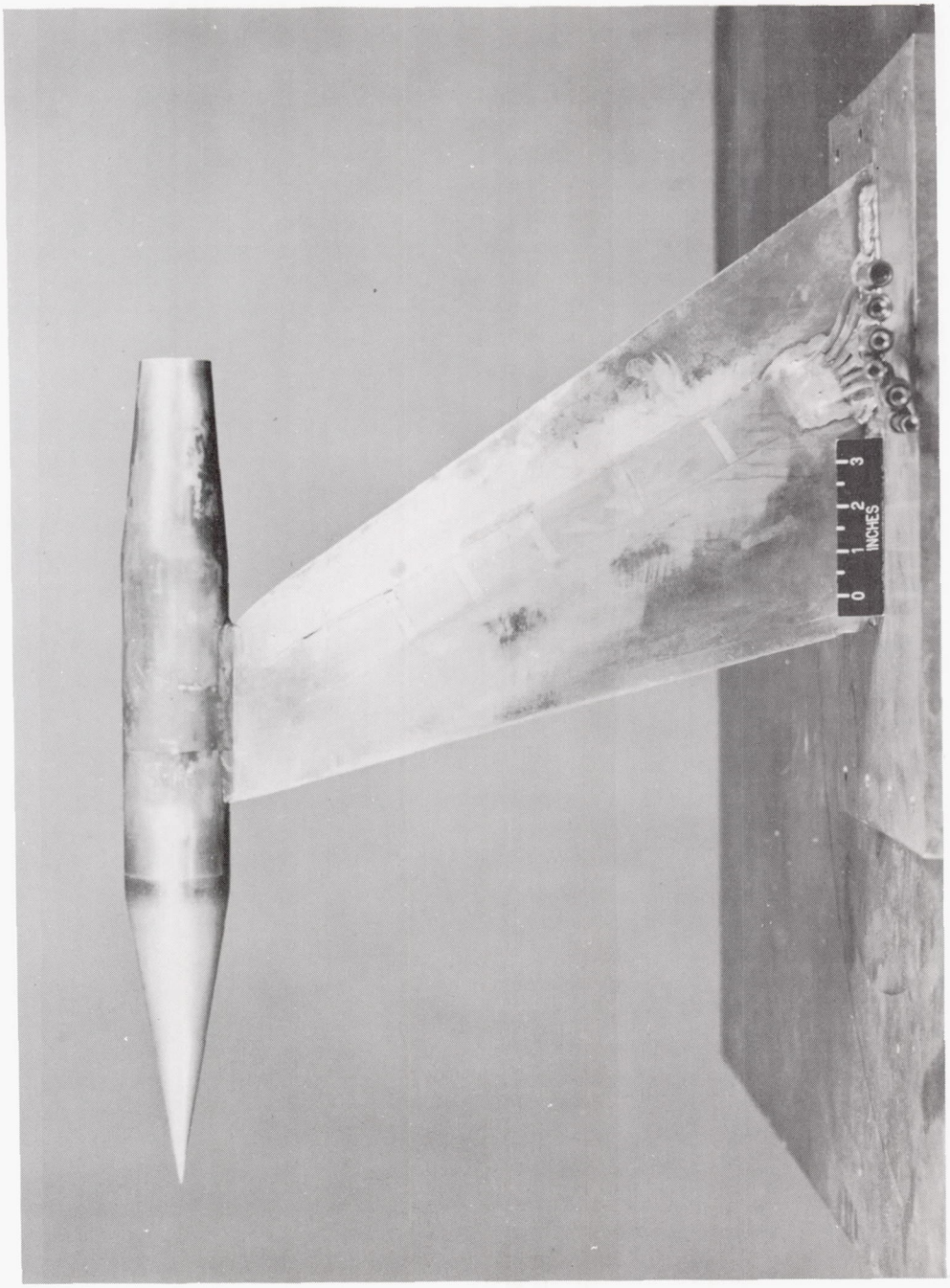

L-83173

(b) Model 2; $\beta = 5^{\circ}$.

Figure 1.- Continued.

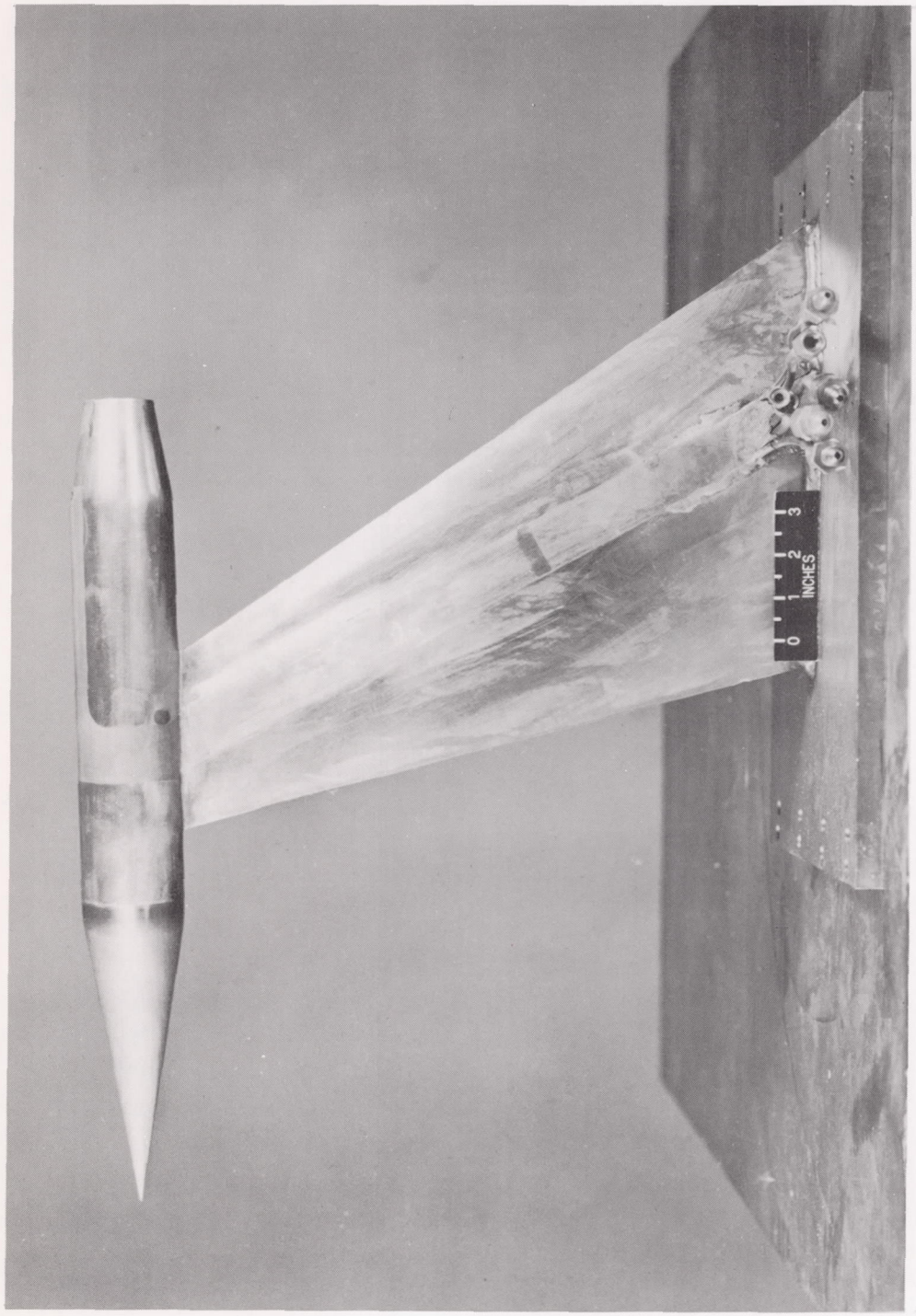

L-83170

(c) Model 3; $\beta = 10^{\circ}$.

Figure 1.- Concluded.

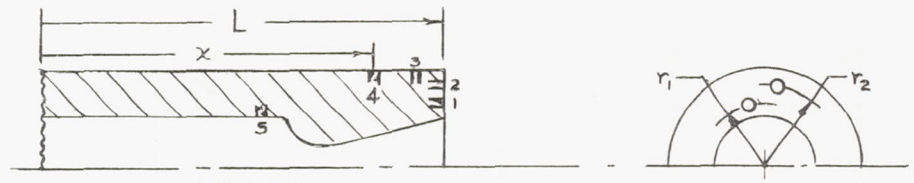

Model 1

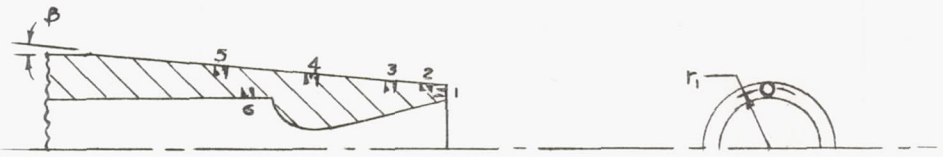

Model 2

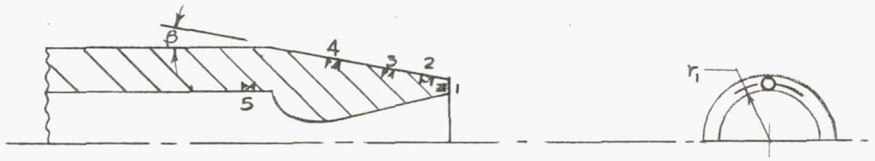

Model 3

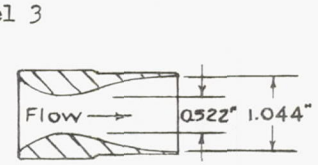

Nozzle 1; M_j = 2.65

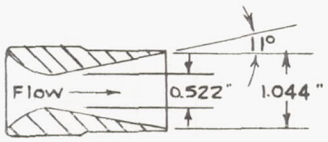

Nozzle 2; M_j = 2.65

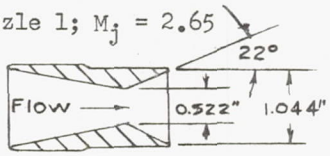

Nozzle 3; M_j = 2.65

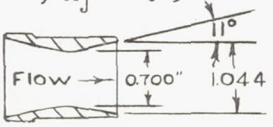

Nozzle 4; M_j = 2.16

Model	β, deg	Orifice	x/L	Radius, in.
1	0	1	1.000	0.670
		2	1.000	0.865
		3	0.992	1.200
		4	0.947	1.200
		5	Combustion chamber	
2	5	1	1.000	0.700
		2	0.991	0.810
		3	0.951	0.880
		4	0.904	0.960
		5	0.818	1.100
		6	Combustion chamber	
3	10	1	1.000	0.700
		2	0.992	0.828
		3	0.950	0.965
		4	0.924	1.120
		5	Combustion chamber	

Figure 2.- Afterbody configurations and jet nozzles.

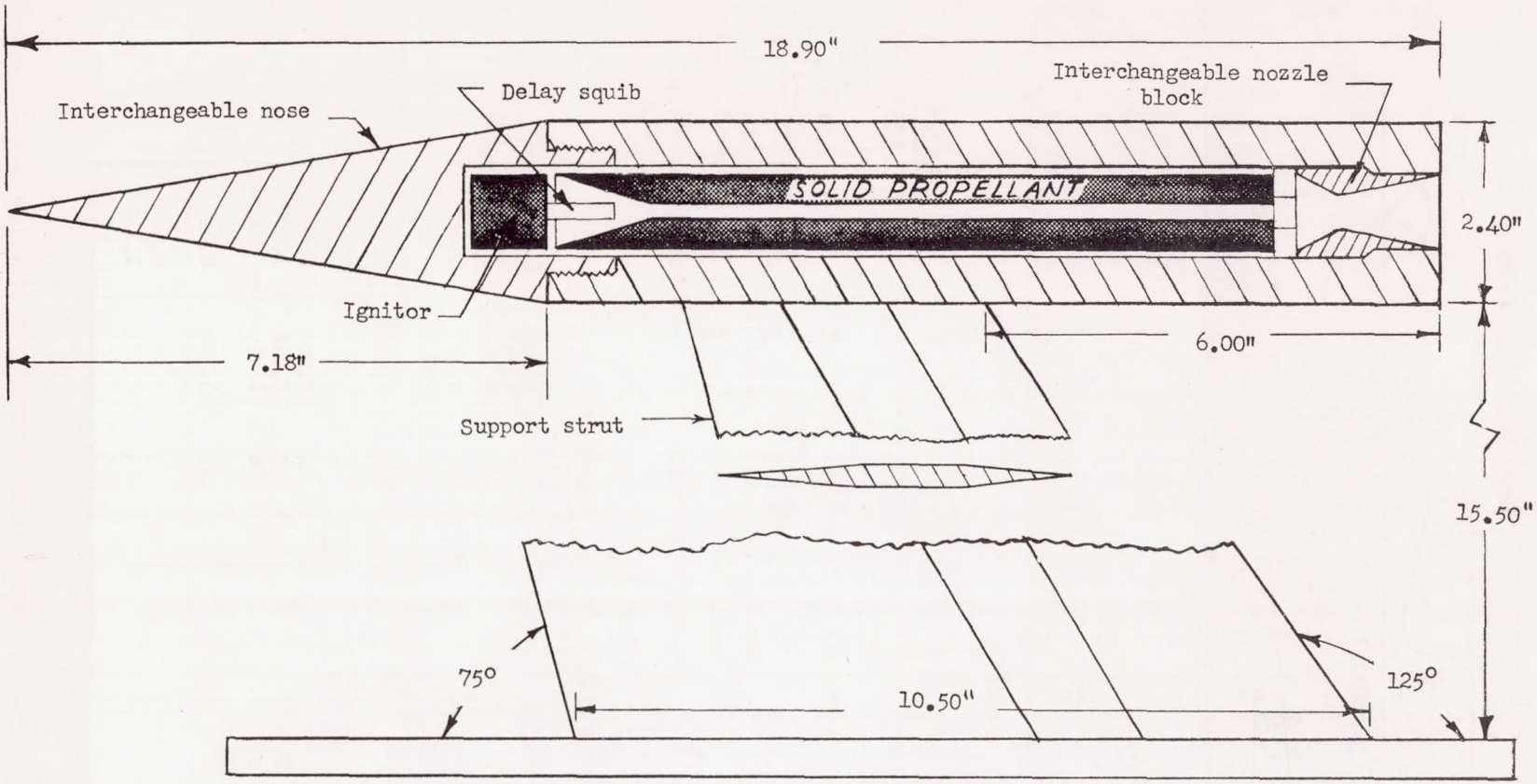

Figure 3.- Assembled model.

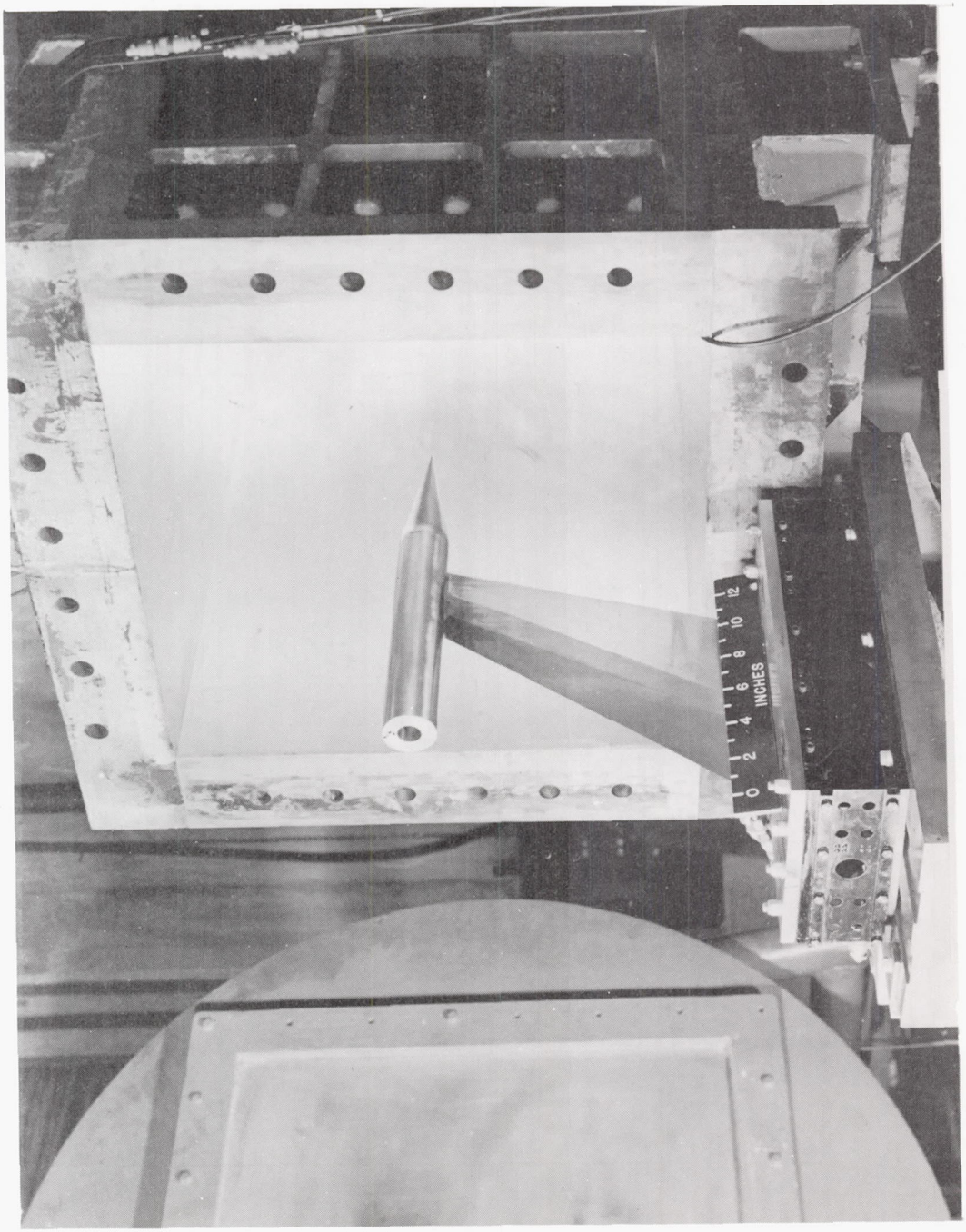

L-73750

Figure 4.- Typical setup.

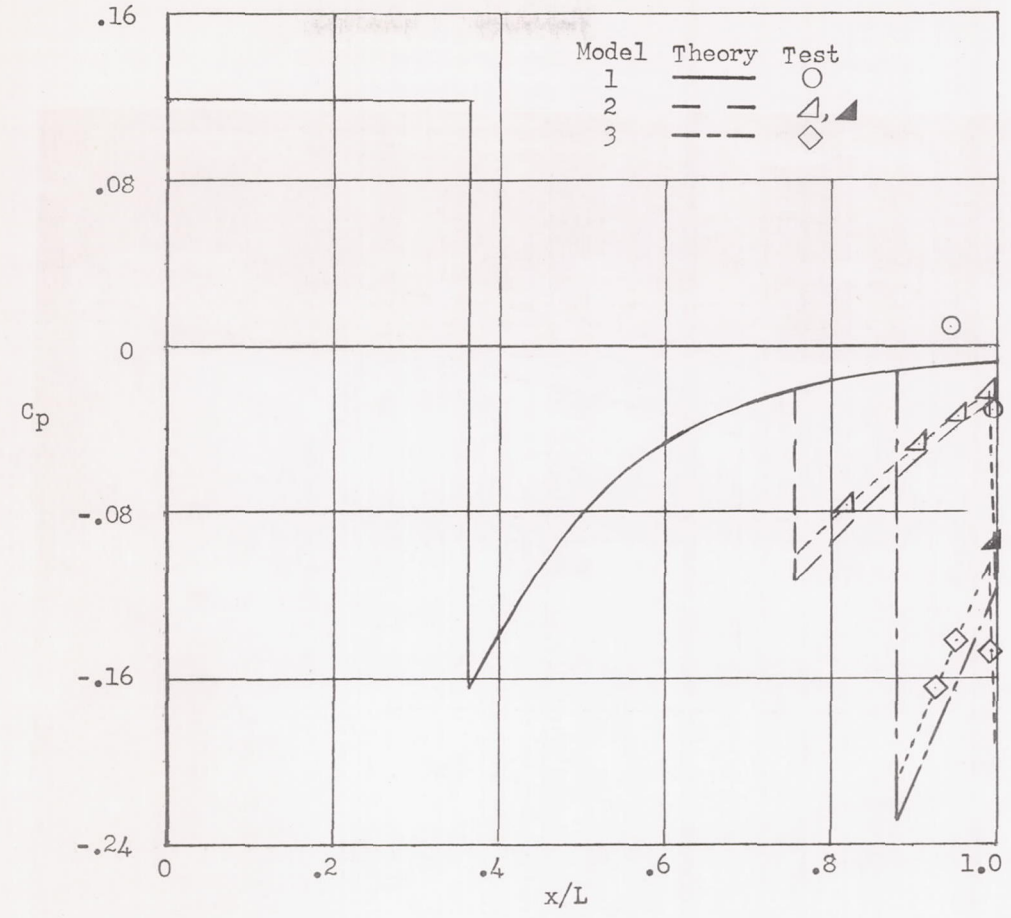

(a) Model pressure distributions.

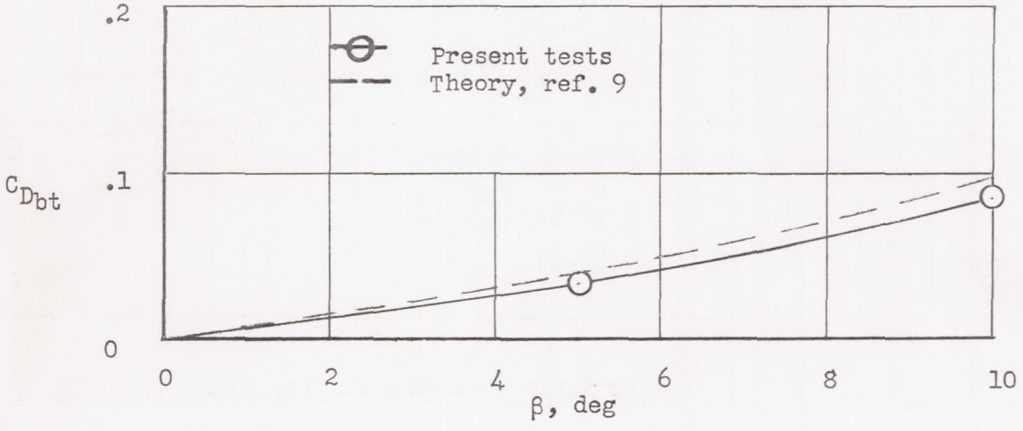

(b) Boattail drag coefficients as a function of boattail angle.

Figure 5.- Power-off boattail pressure distributions and drag coefficients.

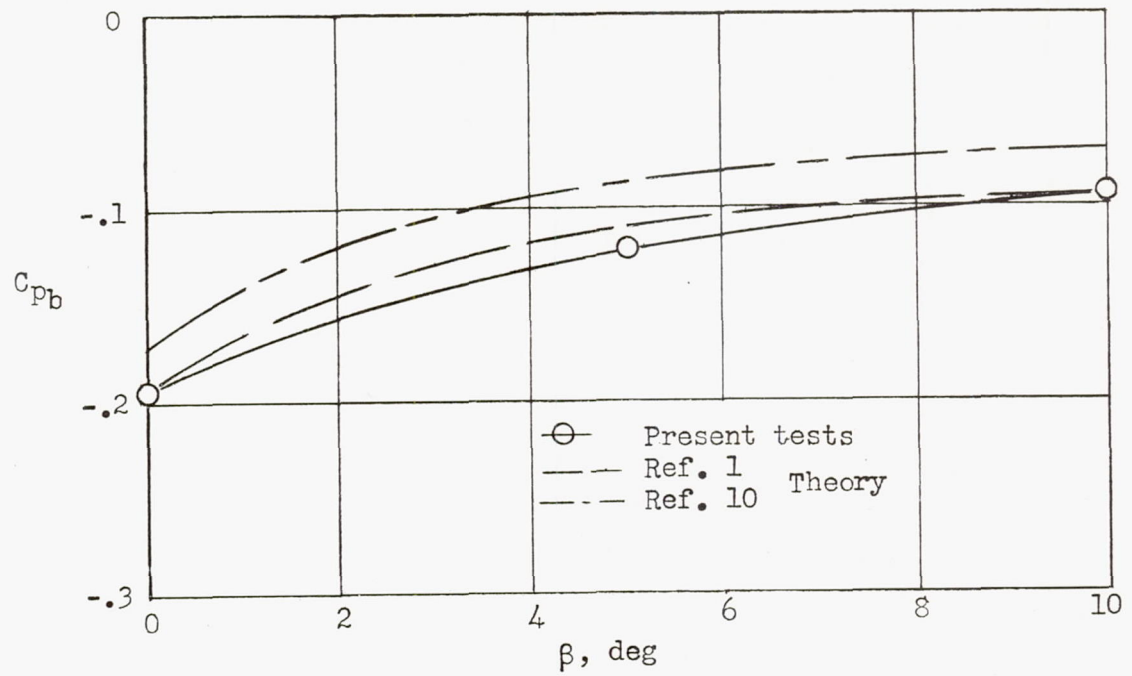

Figure 6.- Base pressure coefficients as a function of boattail angle.

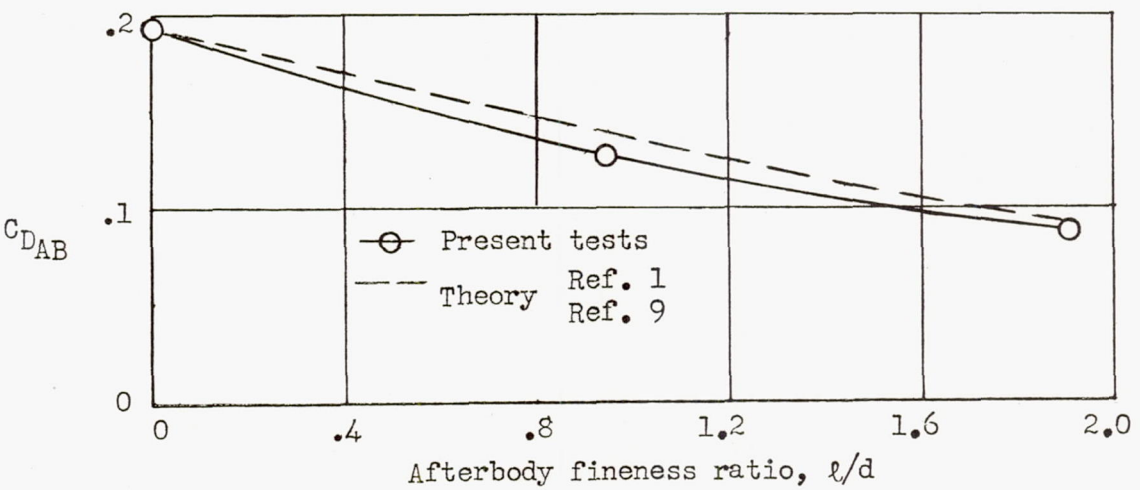

Figure 7.- Afterbody drag coefficient as a function of afterbody fineness ratio.

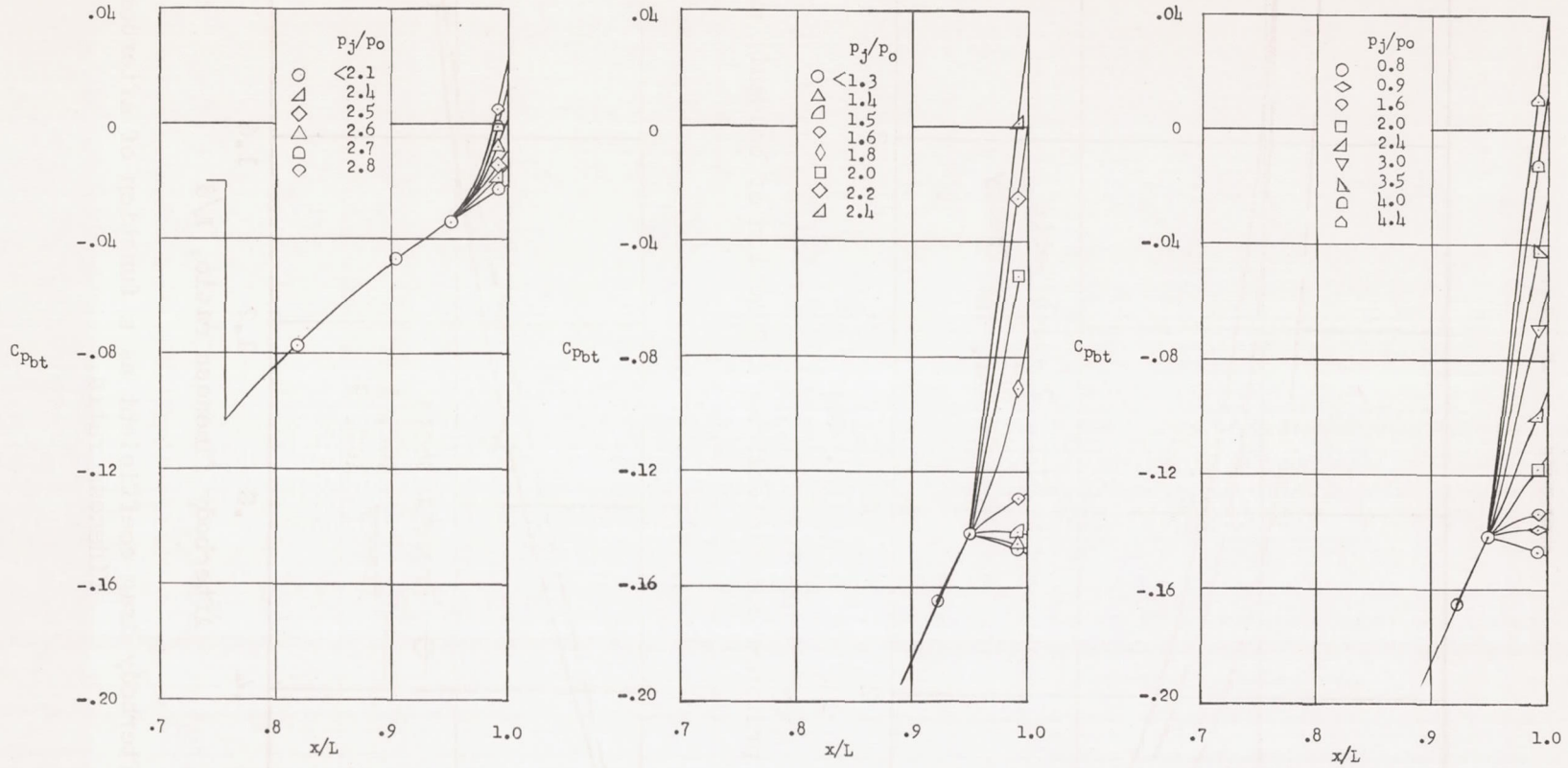

(a) $\beta = 5^\circ$; $\lambda = 22^\circ$; $M_j = 2.65$.

(b) $\beta = 10^\circ$; $\lambda = 22^\circ$; $M_j = 2.65$.

(c) $\beta = 10^\circ$; $\lambda = 11^\circ$; $M_j = 2.16$.

Figure 8.- Jet interference on boattail pressure distributions.

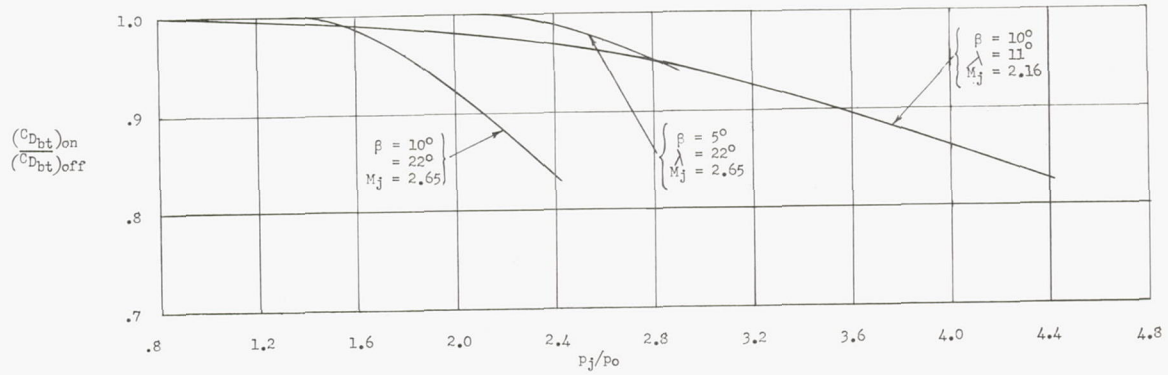

Figure 9.- Reduction in boattail drag due to jet interference effects.

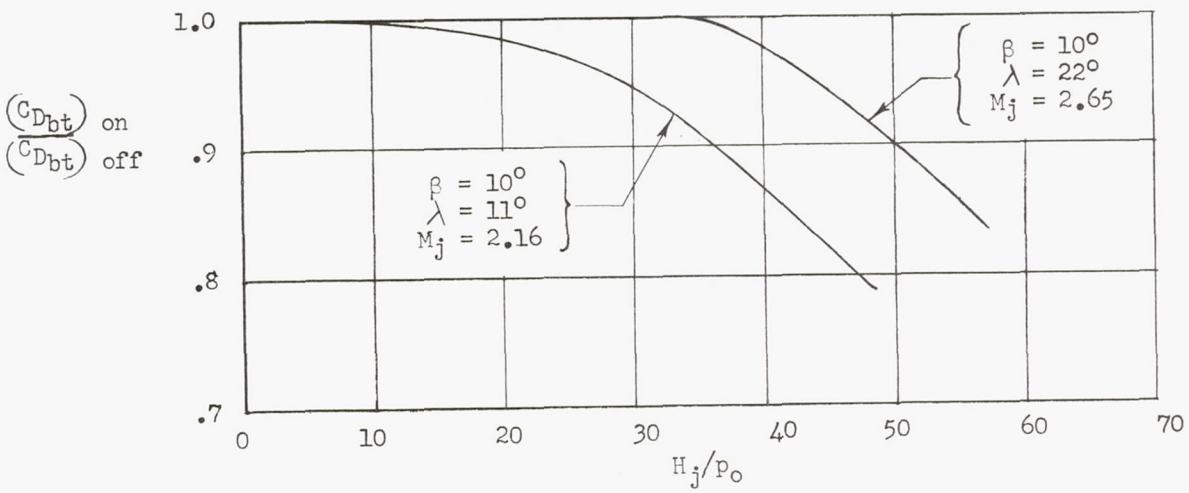

Figure 10.- Reduction in boattail drag as a function of jet total pressure ratio.

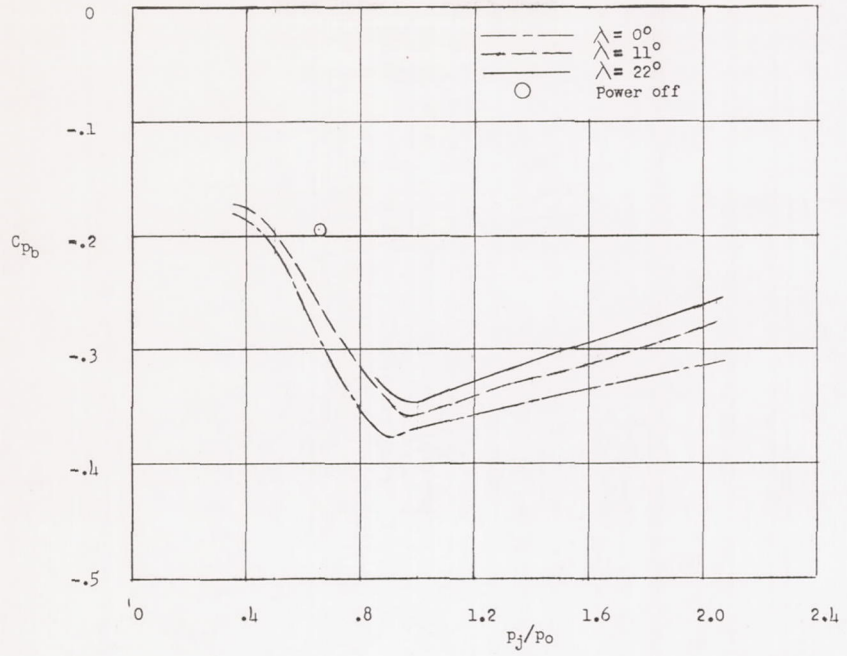

(a) $\beta = 0°$.

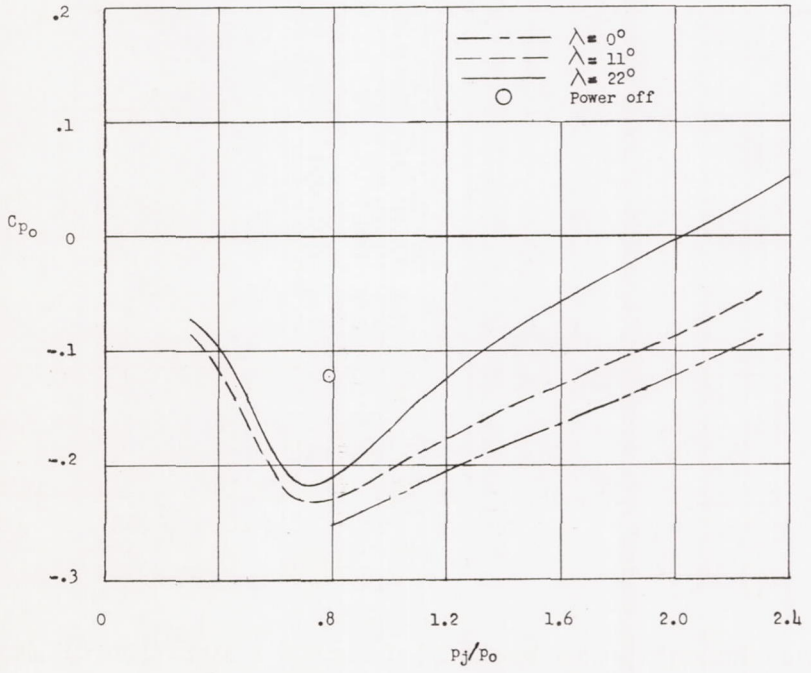

(b) $\beta = 5°$.

Figure 11.- Base pressure coefficient as a function of jet pressure ratio and nozzle half-angle for $M_j = 2.55$.

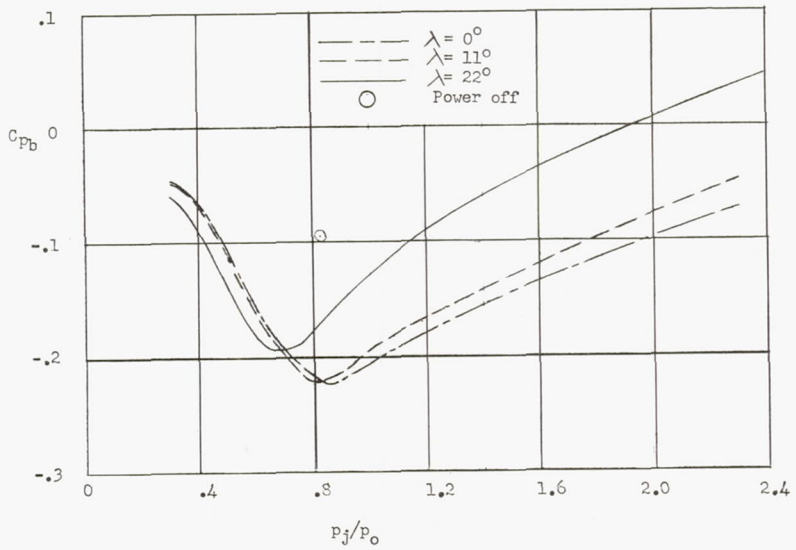

(c) $\beta = 10^\circ$.

Figure 11.- Concluded.

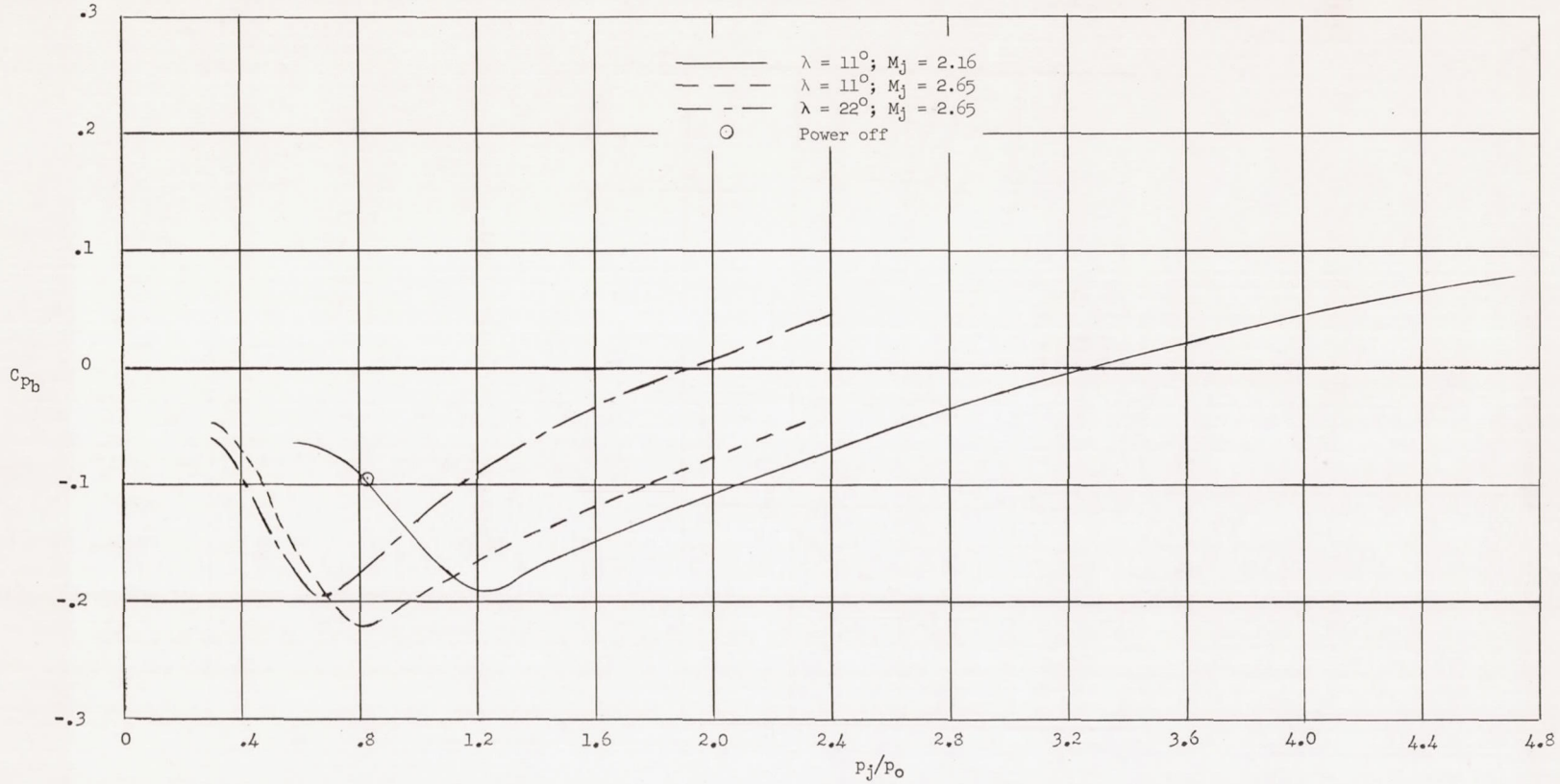

Figure 12.- Base-pressure coefficient for $\beta = 10^{\circ}$ as a function of jet pressure ratio.

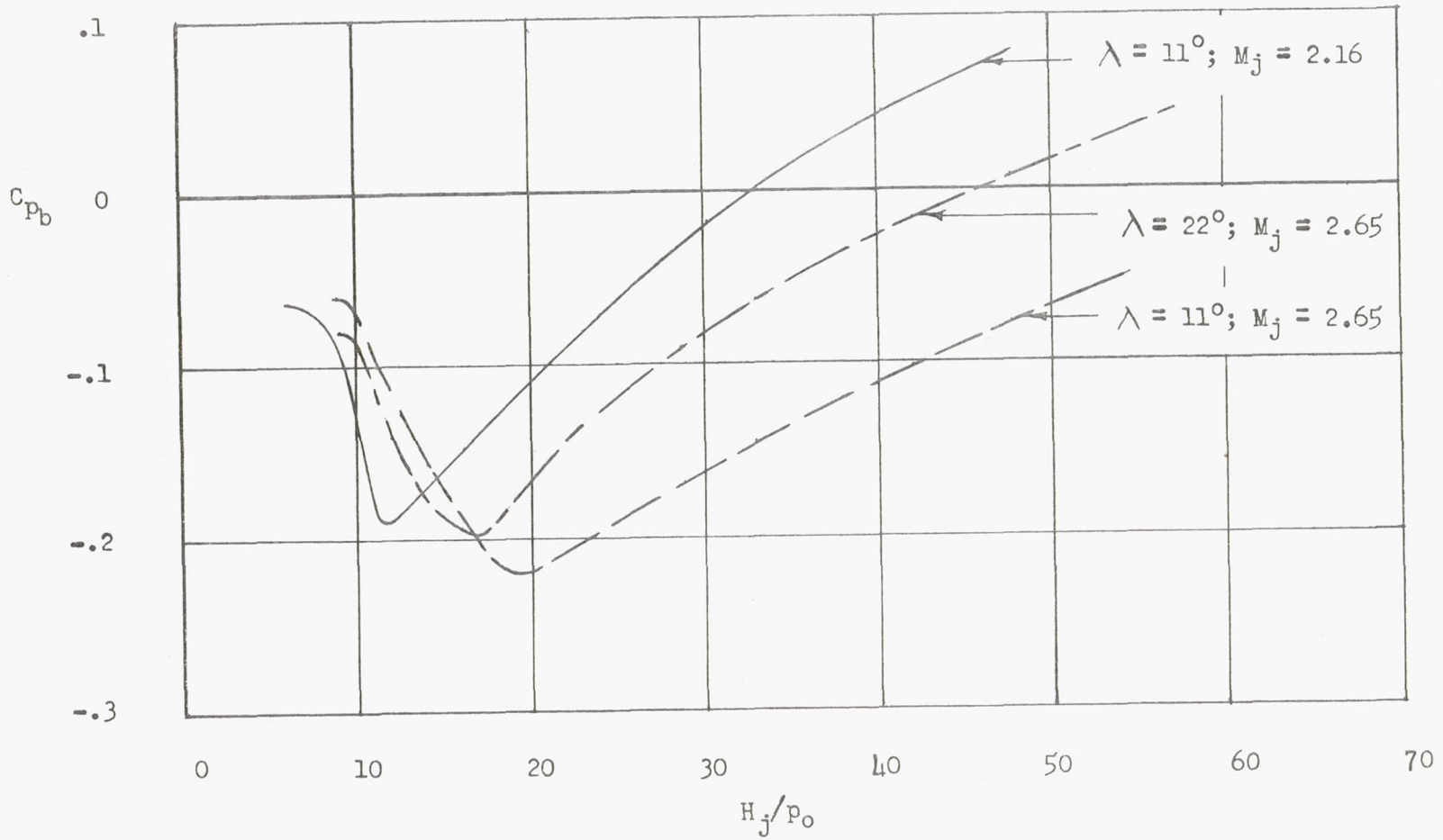

Figure 13.- Base pressure coefficient for $\beta = 10^\circ$ as a function of jet total pressure ratio.

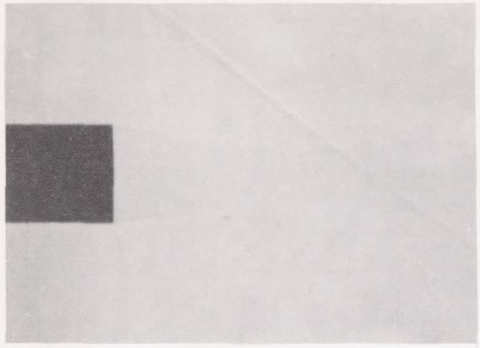

Power off

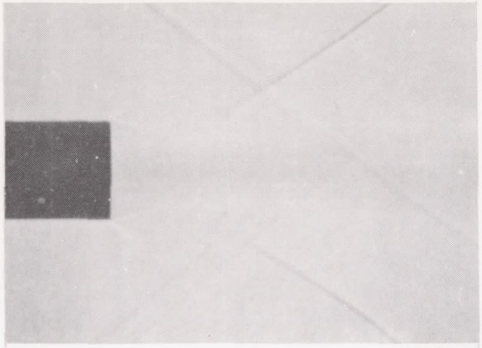

$p_j/p_o = 0.8$

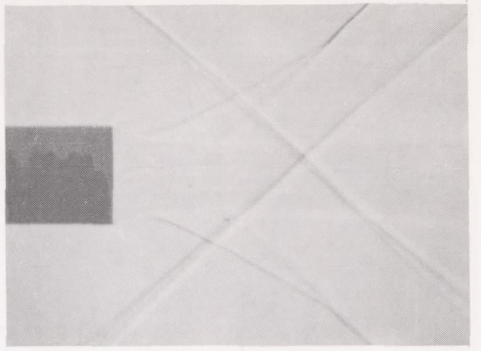

$p_j/p_o = 1.10$

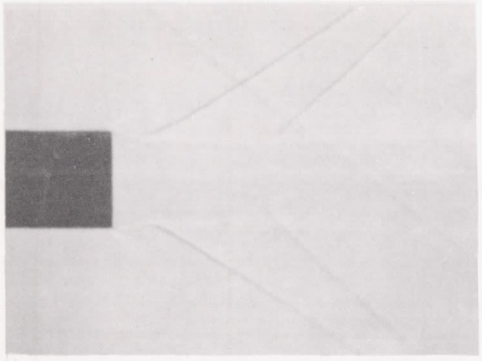

$p_j/p_o = 1.60$

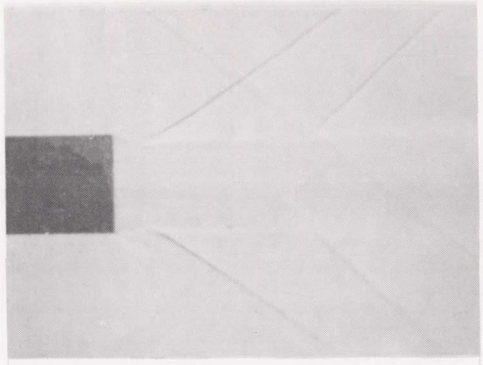

$p_j/p_o = 2.10$

L-83618

(a) $\beta = 0^\circ$; $\lambda = 22^\circ$.

Figure 14.- Shadowgraphs of flow phenomena.

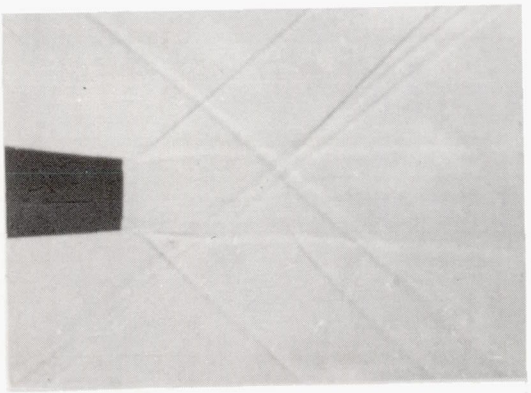

p_j/p_o = 1.60

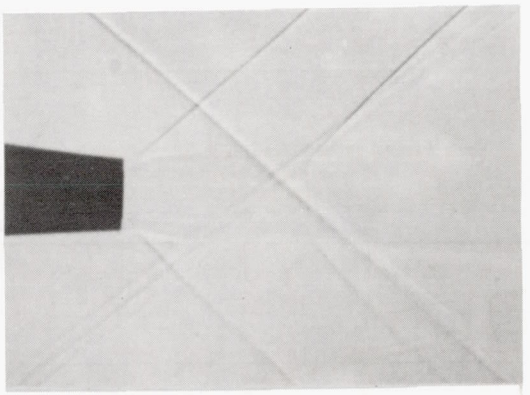

p_j/p_o = 1.80

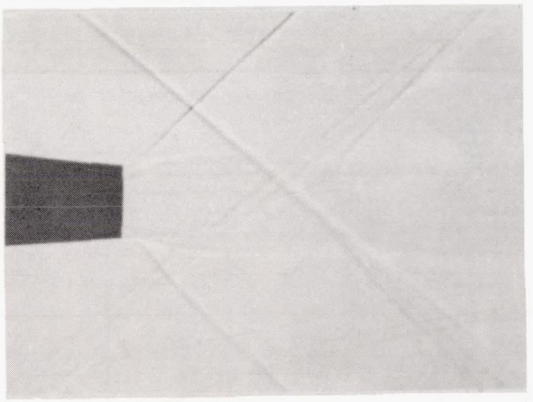

p_j/p_o = 2.20

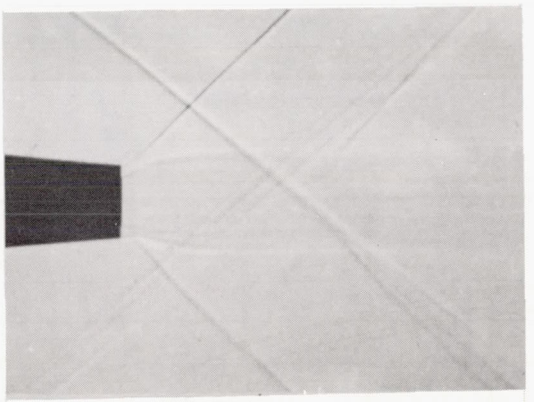

p_j/p_o = 2.40

L-83619

(b) $\beta = 5^\circ$; $\lambda = 22^\circ$.

Figure 14.- Concluded.

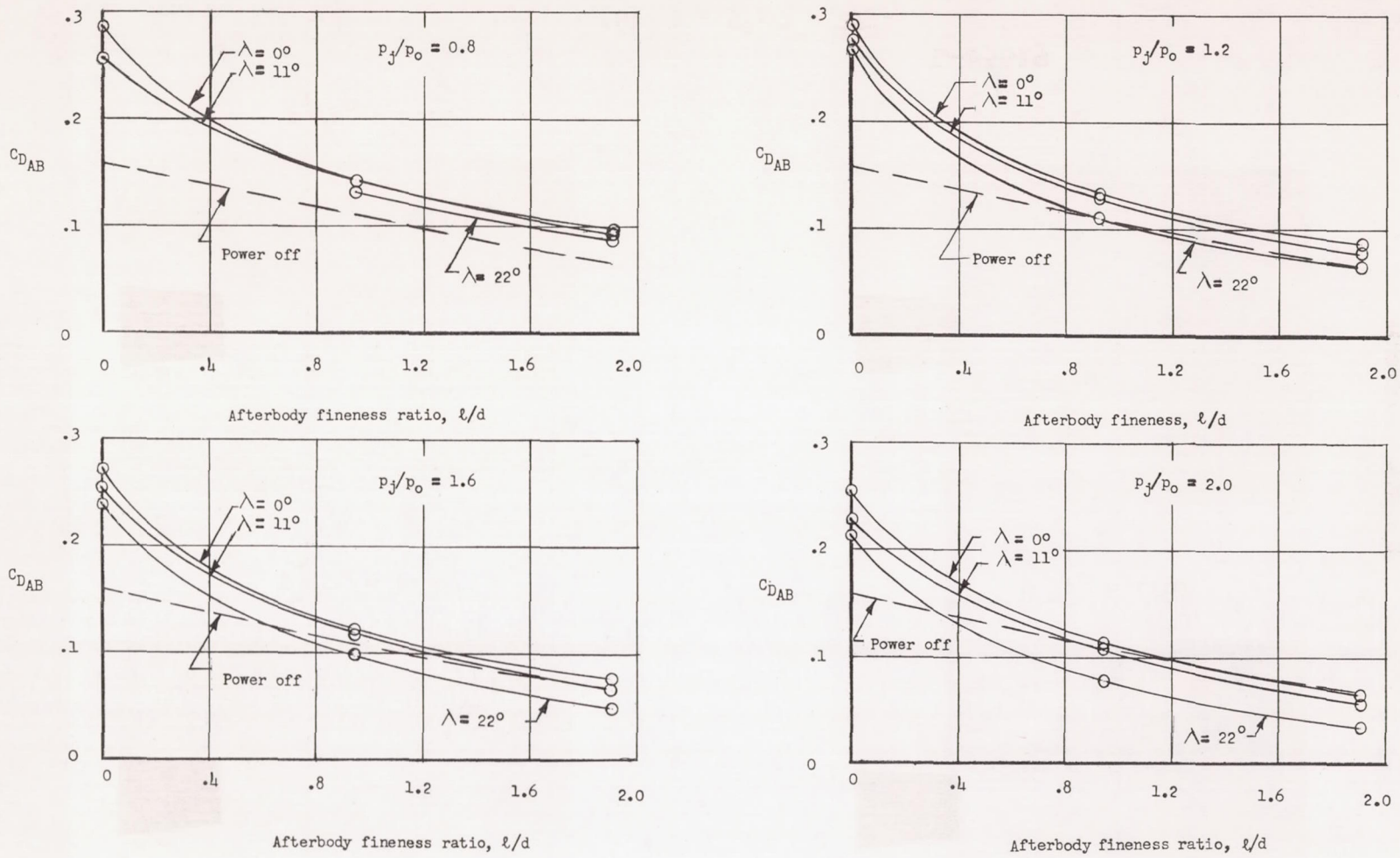

Figure 15.- Afterbody drag coefficient as a function of afterbody fineness ratio and nozzle half-angle for constant values of p_j/p_o and for M_j = 2.65.

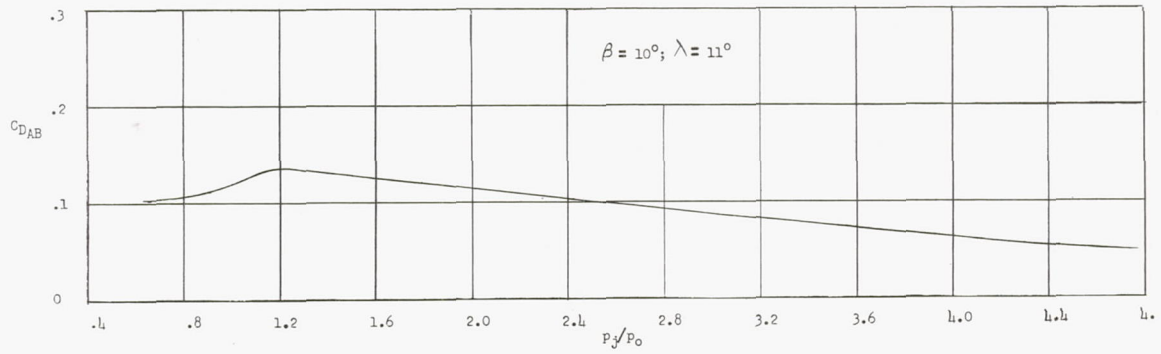

Figure 16.- Afterbody drag coefficient as a function of jet pressure ratio for $M_j = 2.16$.

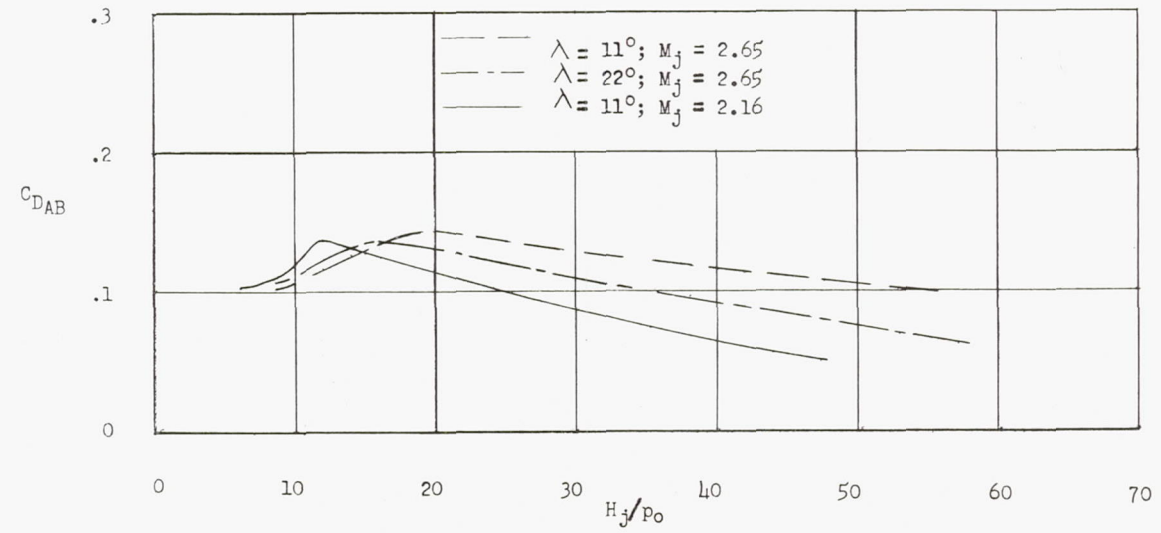

Figure 17.- Afterbody drag coefficient as a function of nozzle half-angle and jet Mach number for model 3 ($\beta = 10°$).